Two-quasiparticle configurations, signature inversion, and the $\pi i_{13/2} \otimes \nu i_{13/2}$ band in ^{176}Ir

R. A. Bark,[1] A. M. Baxter,[2] A. P. Byrne,[1,2] P. M. Davidson,[1] G. D. Dracoulis,[1] S. M. Mullins,[1] T. R. McGoram,[1] and R. T. Newman[1]

[1]*Department of Nuclear Physics, RSPhysSE, Australian National University, Canberra ACT 0200, Australia*

[2]*Department of Physics and Theoretical Physics, Faculty of Science, Australian National University, Canberra ACT 0200, Australia*

(Received 16 October 2002; published 31 January 2003)

High-spin states have been populated in ^{176}Ir using the ^{149}Sm(^{31}P,4n) reaction. Gamma-gamma coincidence techniques have allowed numerous bands up to a maximum spin of 32 to be identified. Configurations have been assigned based on spectroscopic properties such as $B(M1)/B(E2)$ values and aligned angular momenta. Signature inversions are observed in bands based on the $\pi h_{9/2} \otimes \nu i_{13/2}$ and $\pi i_{13/2} \otimes \nu i_{13/2}$ configurations. These inversions are compared with particle-rotor model calculations and are qualitatively reproduced when a residual proton-neutron interaction is included. The shape evolution of the bands has been studied using diabatic potential energy surface calculations. A strong configuration dependence is predicted.

DOI: 10.1103/PhysRevC.67.014320 PACS number(s): 21.10.Tg, 21.10.Hw, 21.90.+f, 27.70.+q

I. INTRODUCTION

In a deformed odd-odd nucleus, the Coriolis force is expected to favor the branch of a two-quasiparticle rotational band having a signature, α_f, given by the proton and neutron angular momenta j_p and j_n: $\alpha_f = \frac{1}{2}[(-1)^{j_p - 1/2} + (-1)^{j_n - 1/2}]$. There is now a body of experimental evidence demonstrating that this rule is violated at low spins, giving rise to a ''signature inversion,'' for certain combinations of proton and neutron orbitals. A well-known configuration exhibiting signature inversion in the rare-earth region is the $\pi h_{11/2} \otimes \nu i_{13/2}$ system. Explanations for this inversion have included Coriolis effects [1], triaxiality [2], proton-neutron (p-n) interactions [3,4] and mixing with the $\pi h_{9/2} \otimes \nu i_{13/2}$ configuration [5]. The inclusion of quadrupole pairing in self-consistent mean-field calculations has also been shown to generate signature inversions [6].

Due to the absence of firm spin assignments in earlier works, it is only recently that signature inversion has been discovered in the $\pi h_{9/2} \otimes \nu i_{13/2}$ bands of the rare-earth region [7]. In these cases, it has been shown that a residual p-n interaction can give a good qualitative account of the inversion [7–10]. A feature of the p-n interaction is that the particle-hole interaction is repulsive while the particle-particle part is attractive. In the rare-earth region, the $\pi h_{9/2}$ orbital is predominantly of particle character, while the $\nu i_{13/2}$ orbital has a quasiparticle character, since it is usually only partially filled. Differences in the particle-hole content of odd and even spin states, due to Coriolis mixing, give rise to a staggering in the strength of the residual interaction, and ultimately affect the signature splitting. Therefore, in this model, signature inversions are possible when a proton particle is coupled to an $i_{13/2}$ quasineutron.

In the rare-earth region, this condition is also expected to be fulfilled by the $\pi i_{13/2} \otimes \nu i_{13/2}$ configuration. Recently, evidence that signature inversion also occurs in this configuration in ^{176}Ir and ^{178}Ir has been reported [11–13]. This work extends the results on the odd-odd nucleus ^{176}Ir in an investigation of signature splitting in the $\pi i_{13/2} \otimes \nu i_{13/2}$ band.

II. EXPERIMENT

A favorable region to search for a $\pi i_{13/2} \otimes \nu i_{13/2}$ band is one in which the one-quasiparticle $\pi i_{13/2}$ bands are known to be low in excitation energy. Systematics [14], in agreement with recent calculations [15], show that the $\pi i_{13/2}$ configuration minimizes in energy near $N=98$ in Re and Ir isotopes and near $N=102$ in Au isotopes. Indeed, the $\pi i_{13/2}$ bands known to have the lowest bandhead energies are in ^{175}Ir and ^{181}Au with $N=98$ and 102, respectively [15–18]. Proton $i_{13/2}$ bands are also known in Re nuclei, but here the $\pi i_{13/2}$ orbital lies further from the Fermi surface, and competing positive-parity three-quasiparticle states can be mistaken for the $\pi i_{13/2}$ band [14]. The $i_{13/2}$ bands are yrast in Au and Tl nuclei near $N=98$, but these nuclei have lower production cross sections due to competition with fission [15,16].

Therefore the nucleus $^{176}Ir_{99}$ was chosen to search for a $\pi i_{13/2} \otimes \nu i_{13/2}$ band. The reaction ^{149}Sm(^{31}P,4n)^{176}Ir was employed in two experiments. In the first, a 158 MeV beam, pulsed 1 ns on and 1.7 μs off, impinged on a 6 mg/cm^2 self-supporting target which was sufficiently thick to stop the recoiling nuclei. In the second, a dc beam of 140 MeV impinged on a 0.9 mg/cm^2 target, which allowed the nuclei to recoil into vacuum, thereby minimizing Doppler broadening effects at high spin. Gamma rays from the reaction were recorded in γ-γ coincidence mode using the CAESAR array, comprising six Compton suppressed HpGe detectors and two low energy photon spectrometer (LEPS) detectors. Two of the HPGe detectors are located at 97° to the beam axis, two at 48°, and two at 145°.

The data were sorted into two-dimensional γ-γ matrices subject to various time conditions, which were then analyzed to construct the decay scheme using the RADWARE package [19]. DCO ratios were formed as described in Ref. [20], as the ratio of coincidence intensity for two γ rays, γ_1 and γ_2, detected at 48°/145° and 97°, respectively, to the coincidence intensity of γ_1 and γ_2 detected at 97° and 48°/145°, respectively.

For gates (γ_2) on stretched quadrupole transitions, the DCO ratios are expected to be unity for stretched quadrupole transitions, (γ_1), and 0.6 for pure stretched dipole transi-

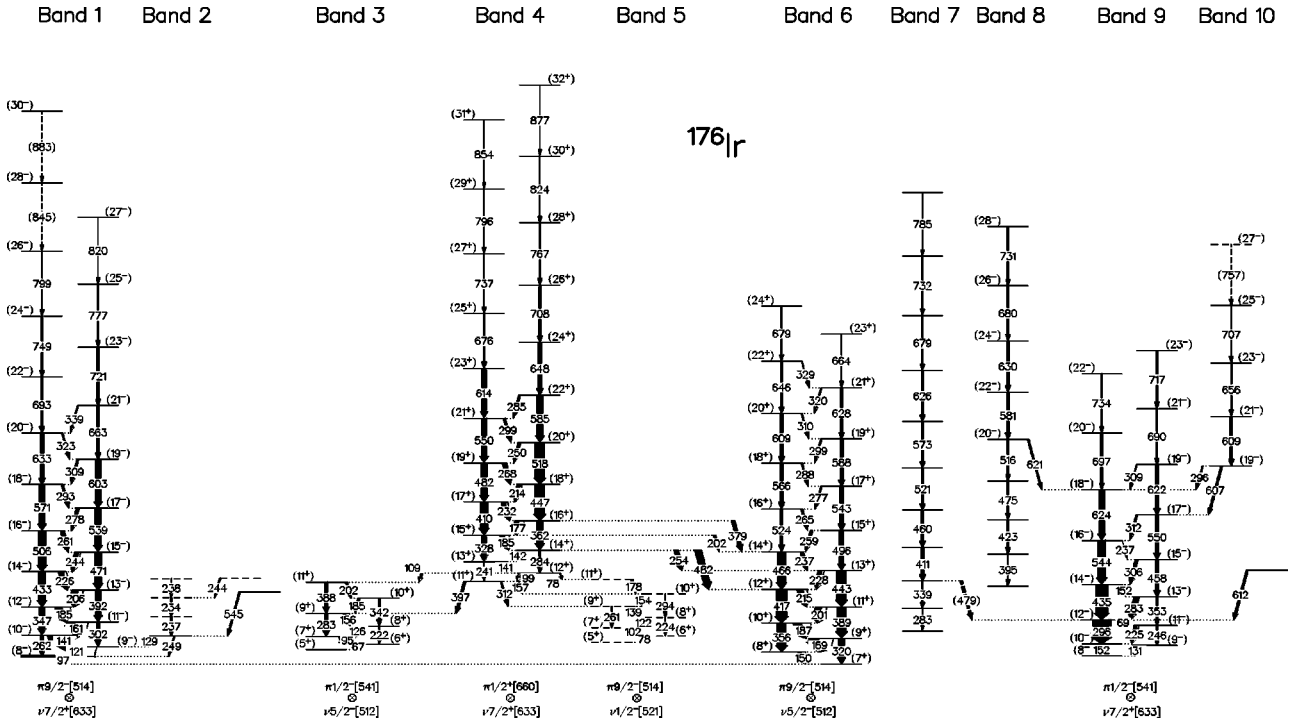

FIG. 1. Level scheme of ^{176}Ir deduced in the present work.

tions, (γ_1). For mixed dipole transitions, DCO ratios less than 0.6 imply negative mixing ratios and those greater than 0.6, positive mixing ratios.

III. RESULTS

The level scheme determined in this work, with bands labeled numerically, is shown in Fig. 1. The present level scheme extends the work of Zhang *et al.* [13] with the observation of six new bands. Only bands 1, 4, 6, and 9 were reported previously and these have been extended to higher spins, and in the case of band 9, possibly also to lower spins. Gamma rays assigned to ^{176}Ir, and their properties, are listed in Table I. The coincidence intensities listed in the table were deduced from the recoil-into-vacuum γ-γ matrix, using the code ESCL8R [19]. Because only a little of ^{176}Ir is known from decay studies [21,22], a discussion of the assignment of spins and parities is deferred to the next section, where the likely configuration assignments are considered. Where the level schemes overlap, the present assignments are in agreement with Zhang *et al.* [13].

Coincidence spectra obtained from the recoil-into-vacuum data, shown in Fig. 2, demonstrate the lines belonging to the most strongly populated bands. Transitions belonging to band 1 can be seen in Fig. 2(a), obtained by gating on the 97 keV transition, which is placed depopulating the band. This transition has an internal conversion coefficient [23], deduced from the intensity balance at the (8^-) level in the 141 keV coincidence gate, of 0.51(14), which is in good agreement with the theoretical conversion coefficient for an $E1$ multipolarity ($\alpha_{E1}=0.431$, $\alpha_{M1}=6.96$, $\alpha_{E2}=5.26$). It decays with a measured mean life of 4.1 ± 0.5 ns, determined from the thick target data, which can be judged from the centroid shift shown in Fig. 3. Although we attribute this mean life to the head of band 1, it is possible that the bandhead actually decays by unobserved transitions to another level that emits the 97 keV gamma ray. In Fig. 2(a), transitions belonging to band 8 are also visible, but the path to the 97 keV transition could not be determined. The 97 keV transition is nevertheless tentatively assigned as the (8^-) $\rightarrow(7^+)$ decay from the head of band 1 to the head of band 6 as discussed further in Sec. IV C 4. Also visible in Fig. 2(a) are gamma rays associated with the levels labeled as band 2, which feed band 1. The ordering of the higher-lying levels of band 2 could not be confirmed.

The spectrum shown in Fig. 2(b) is formed by summing the 482 and 447 keV coincidence gates together. Transitions of these energies are placed in band 4, which is linked to bands 3, 5, and 6. The transitions which link band 4 to bands 3 and 6 presumably arise due to mixing caused by the near degeneracy of pairs of levels at (11^+) and (14^+). The link to band 5 is uncertain due to insufficient statistics — the 78 keV transition, joining bands 4 and 5 together, might also, or alternatively, be placed at the bottom of band 5. Indeed, due to the low energy (<100 keV) of transitions placed near the bottom of bands 3–5, and the accompanying high internal conversion and low detection efficiency, it is not certain whether transitions of even lower energy exist in these bands and therefore that the heads of these bands have been identified. In contrast, for band 6, the regular decrease in transition energies below spin (13^+) implies that the next dipole transition below the 150 keV line, if it existed, would have an energy near 130 keV. Because no such line is visible in the spectrum shown in Fig. 2(b), the head of band 6 is regarded as established.

Figure 2(c) is obtained by gating on the 296 keV line, and

TABLE I. Gamma rays assigned to ^{176}Ir.

E_γ [a] (keV)	I_γ	E_i [b] (keV)	E_f [b] (keV)	$J_i^\pi(\hbar)$	$J_f^\pi(\hbar)$	DCO
53.04(2) [c]						
55.49(2) [c]						
56.77(2) [c]						
61.53(2) [c]						
67.00(100)		247.6(6)	180.6	(6^+)	(5^+)	
69.17(5)	<5	447.3(3) [d]	377.4 [d]	(12^-)	(11^-)	
69.42(1) [c]						
78.40(100)		348.1(7)	269.7	(6^+)	(5^+)	
78.45(100)	0.2(1)	1122.2(4)	1043.5	(12^+)	(11^+)	
95.12(4)	7.2(7)	342.8(5)	247.6	(7^+)	(6^+)	
97.26(3)		97.3(2)	0.0	(8^-)	(7^+)	0.50(7)
99.30(10)	1.1(2)	1122.2(4)	1022.7	(12^+)	(11^+)	
102.13(4)	0.8(16)	450.2(7)	348.1	(7^+)	(6^+)	
108.92(5)	1.2(2)	1122.2(4)	1013.3	(12^+)	(11^+)	
120.74(3)		218.2(3)	97.3	(9^-)	(8^-)	
121.78(4)	5.6(7)	572.0(6)	450.2	(8^+)	(7^+)	
126.12(4)	8.6(6)	469.1(5)	342.8	(8^+)	(7^+)	
129.45(10)	2.5(3)	346.0(0)	218.2		(9^-)	
131.00(3)		131.0(2) [d]	0.0 [d]	(9^-)	(8^-)	0.35(7)
139.01(4)	5.9(5)	711.0(6)	572.0	(9^+)	(8^+)	
140.54(3)	34.7(11)	359.0(3)	218.2	(10^-)	(9^-)	0.62(23)
140.97(4)	9.0(4)	1263.3(3)	1122.2	(13^+)	(12^+)	0.35(16) [e]
141.87(4)	6.8(3)	1405.5(3)	1263.3	(14^+)	(13^+)	0.35(16) [e]
150.18(3)		150.3(2)	0.0	(8^+)	(7^+)	1.06(13)
151.95(4)		151.9(2) [d]	0.0 [d]	(10^-)	(8^-)	1.10(20)
152.03(18)	1.2(2)	882.6(3) [d]	730.5 [d]	(14^-)	(13^-)	
154.47(4)	7.2(4)	865.5(6)	711.0	(10^+)	(9^+)	
156.15(4)	8.9(4)	625.6(5)	469.1	(9^+)	(8^+)	
157.17(6)	3.3(2)	1022.7(5)	865.5	(11^+)	(10^+)	
160.88(3)	32.1(10)	520.2(3)	359.0	(11^-)	(10^-)	0.68(13)
168.84(3)	40.4(14)	319.4(2)	150.3	(9^+)	(8^+)	0.98(12)
176.85(3)	16.8(6)	1768.0(3)	1591.0	(16^+)	(15^+)	
178.00(20)	3.9(3)	1043.5(13)	865.5	(11^+)	(10^+)	
185.19(3)	17.4(6)	1591.0(3)	1405.5	(15^+)	(14^+)	
185.26(5)	4.9(4)	811.1(5)	625.6	(10^+)	(9^+)	0.39(14)
185.36(3)	29.5(10)	705.8(4)	520.2	(12^-)	(11^-)	0.66(11)
187.03(3)	33.0(11)	506.6(2)	319.4	(10^+)	(9^+)	1.13(15)
201.18(3)	24.6(8)	708.0(2)	506.6	(11^+)	(10^+)	
201.80(7)	4.5(2)	1591.0(3)	1389.0	(15^+)	(14^+)	
201.98(5)	5.3(3)	1013.3(5)	811.1	(11^+)	(10^+)	
206.27(3)	25.1(8)	912.3(4)	705.8	(13^-)	(12^-)	0.80(18)
213.93(4)	11.6(4)	2214.5(3)	2000.4	(18^+)	(17^+)	0.81(24)
215.18(3)	23.1(8)	923.3(2)	708.0	(12^+)	(11^+)	1.03(17)
221.62(10)	3.3(4)	469.1(5)	247.6	(8^+)	(6^+)	
224.30(100)	0.9(3)	572.0(6)	348.1	(8^+)	(6^+)	
225.18(4)	12.1(7)	377.4(2) [d]	151.9 [d]	(11^-)	(10^-)	0.71(46)
226.24(3)	19.7(6)	1138.8(4)	912.3	(14^-)	(13^-)	
228.04(4)	14.8(5)	1151.6(3)	923.3	(13^+)	(12^+)	0.54(11)
232.20(3)	16.3(6)	2000.4(3)	1768.0	(17^+)	(16^+)	0.42(16)
233.88(8)	3.5(3)	817.5(0)	583.5			
237.17(12)	4.5(4)	583.5(0)	346.0			
237.46(4)	8.6(3)	1389.0(3)	1151.6	(14^+)	(13^+)	
237.76(20)	1.5(2)	1055.1(0)	817.5			

TABLE I. (*Continued*).

E_γ [a] (keV)	I_γ	E_i [b] (keV)	E_f [b] (keV)	$J_i^\pi(\hbar)$	$J_f^\pi(\hbar)$	DCO
240.98(10)	3.3(2)	1263.3(3)	1022.7	(13^+)	(11^+)	
243.53(12)	3.4(2)	1061.0(0)	817.5			
244.16(3)	16.5(6)	1383.2(4)	1138.8	(15^-)	(14^-)	
246.15(6)	5.5(4)	377.4(2) [d]	131.0 [d]	(11^-)	(9^-)	
248.64(12)	3.5(4)	346.0(0)	97.3		(8^-)	
250.38(4)	7.2(3)	2732.8(4)	2482.4	(20^+)	(19^+)	
253.82(4)	11.8(4)	1405.5(3)	1151.6	(14^+)	(13^+)	
259.42(4)	7.5(4)	1648.1(3)	1389.0	(15^+)	(14^+)	
260.80(20)	3.9(4)	711.0(6)	450.2	(9^+)	(7^+)	
260.92(4)	10.5(4)	1644.6(4)	1383.2	(16^-)	(15^-)	
261.97(5)	10.0(5)	359.0(3)	97.3	(10^-)	(8^-)	
265.15(5)	5.2(3)	1913.2(4)	1648.1	(16^+)	(15^+)	
267.82(4)	12.5(4)	2482.4(4)	2214.5	(19^+)	(18^+)	0.29(10)
277.37(8)	3.3(2)	2190.8(4)	1913.2	(17^+)	(16^+)	
277.70(4)	8.4(3)	1922.6(4)	1644.6	(17^-)	(16^-)	
282.88(5)	0.1(10)	588.1(3) [d]	305.3 [d]			
283.11(4)	13.5(7)	625.6(5)	342.8	(9^+)	(7^+)	
283.18(4)	15.8(6)	730.5(3) [d]	447.3 [d]	(13^-)	(12^-)	0.41(9)
283.58(30)	5.6(3)	1405.5(3)	1122.2	(14^+)	(12^+)	
284.76(5)	5.3(3)	3317.5(4)	3032.4	(22^+)	(21^+)	
288.43(6)	4.2(2)	2479.4(4)	2190.8	(18^+)	(17^+)	
293.30(5)	6.2(3)	2216.0(5)	1922.6	(18^-)	(17^-)	
294.23(32)	2.3(3)	865.5(6)	572.0	(10^+)	(8^+)	
295.64(3)	66.9(23)	447.3(3) [d]	151.9 [d]	(12^-)	(10^-)	0.79(9)
295.88(9)	3.1(2)	2346.2(5) [d]	2050.9 [d]	(19^-)	(18^-)	
298.80(8)	3.7(2)	2778.5(4)	2479.4	(19^+)	(18^+)	
299.32(5)	6.5(3)	3032.4(4)	2732.8	(21^+)	(20^+)	
302.13(4)	10.8(4)	520.2(3)	218.2	(11^-)	(9^-)	
306.01(4)	8.9(4)	1288.7(3)	982.6	(15^-)	(14^-)	0.42(12)
309.25(5)	5.5(3)	2525.4(5)	2216.0	(19^-)	(18^-)	
309.46(10)	2.2(2)	2360.7(5) [d]	2050.9 [d]	(19^-)	(18^-)	
309.63(8)	3.0(2)	3087.8(5)	2778.5	(20^+)	(19^+)	
311.79(5)	5.0(3)	1738.9(4) [d]	1427.0 [d]	(17^-)	(16^-)	
311.84(10)	4.9(3)	1022.7(5)	711.0	(11^+)	(9^+)	
319.62(9)	3.1(3)	3406.5(5)	3087.8	(21^+)	(20^+)	
319.69(4)	21.2(9)	319.4(2)	0.0	(9^+)	(7^+)	
323.48(6)	4.2(2)	2849.1(5)	2525.4	(20^-)	(19^-)	
327.98(4)	18.6(7)	1591.0(3)	1263.3	(15^+)	(13^+)	1.09(46)
329.31(13)	1.9(2)	3734.8(7)	3406.5	(22^+)	(21^+)	
338.53(5)	5.0(2)	926.7(4) [d]	588.1 [d]			
339.20(9)	2.9(2)	3188.3(6)	2849.1	(21^-)	(20^-)	
341.99(7)	6.6(5)	811.1(5)	469.1	(10^+)	(8^+)	
346.79(4)	20.9(8)	705.8(4)	359.0	(12^-)	(10^-)	
353.38(7)	5.9(4)	730.5(3) [d]	377.4 [d]	(13^-)	(11^-)	
356.42(3)	33.3(11)	506.6(2)	150.3	(10^+)	(8^+)	1.02(16)
362.49(3)	25.3(8)	1768.0(3)	1405.5	(16^+)	(14^+)	1.20(24)
379.01(4)	13.1(5)	1768.0(3)	1389.0	(16^+)	(14^+)	
387.85(4)	11.9(6)	1013.3(5)	625.6	(11^+)	(9^+)	
388.76(3)	35.0(12)	708.0(2)	319.4	(11^+)	(9^+)	0.74(12)
392.12(4)	21.3(7)	912.3(4)	520.2	(13^-)	(11^-)	1.46(46)
395.35(6)	3.3(3)	1258.7(5) [d]	863.4 [d]			
397.23(4)	9.2(5)	1022.7(5)	625.6	(11^+)	(9^+)	
409.51(3)	28.6(10)	2000.4(3)	1591.0	(17^+)	(15^+)	

TABLE I. (*Continued*).

E_γ [a] (keV)	I_γ	E_i [b] (keV)	E_f [b] (keV)	$J_i^\pi(\hbar)$	$J_f^\pi(\hbar)$	DCO
411.06(5)	12.8(6)	1337.7(5) [d]	926.7 [d]			
416.79(3)	43.5(14)	923.3(2)	506.6	(12^+)	(10^+)	
422.53(7)	4.6(4)	1681.2(5) [d]	1258.7 [d]			
433.00(3)	27.3(9)	1138.8(4)	705.8	(14^-)	(12^-)	
435.24(3)	47.9(16)	882.6(3) [d]	447.3 [d]	(14^-)	(12^-)	1.28(15)
443.50(3)	36.0(12)	1151.6(3)	708.0	(13^+)	(11^+)	
446.65(3)	37.4(12)	2214.5(3)	1768.0	(18^+)	(16^+)	0.88(17)
458.20(5)	12.8(5)	1188.7(3) [d]	730.5 [d]	(15^-)	(13^-)	
460.00(20)	9.6(4)	1797.7(13) [d]	1337.7 [d]			
465.72(3)	29.5(10)	1389.0(3)	923.3	(14^+)	(12^+)	
470.94(4)	27.4(9)	1383.2(4)	912.3	(15^-)	(13^-)	
474.71(7)	5.8(4)	2156.1(5) [d]	1681.2 [d]			
479.36(100)	9.7(5)	1026.7(4) [d]	547.3 [d]		(12^-)	0.86(30)
481.97(4)	25.9(9)	2482.4(4)	2000.4	(19^+)	(17^+)	0.77(15)
482.33(4)	25.6(9)	1405.5(3)	923.3	(14^+)	(12^+)	
496.49(4)	17.4(7)	1648.1(3)	1151.6	(15^+)	(13^+)	0.99(18)
505.95(4)	28.6(10)	1644.6(4)	1138.8	(16^-)	(14^-)	0.84(20)
516.25(7)	4.1(3)	2672.4(6) [d]	2156.1 [d]	(20^-)		
518.44(3)	36.0(12)	2732.8(4)	2214.5	(20^+)	(18^+)	0.99(13)
521.16(6)	8.6(4)	2318.9(14) [d]	1797.7 [d]			
523.96(6)	10.0(4)	1913.2(4)	1389.0	(16^+)	(14^+)	
539.41(4)	23.6(8)	1922.6(4)	1383.2	(17^-)	(15^-)	
542.82(5)	14.8(6)	2190.8(4)	1648.1	(17^+)	(15^+)	
544.40(3)	30.1(10)	1427.0(4) [d]	882.6 [d]	(16^-)	(14^-)	1.06(11)
544.69(21)	5.7(6)	891.1(10)	346.0			
549.97(4)	22.7(8)	3032.4(4)	2482.4	(21^+)	(19^+)	
550.19(5)	12.3(5)	1738.9(4) [d]	1188.7 [d]	(17^-)	(15^-)	
566.04(6)	10.6(5)	2479.4(4)	1913.2	(18^+)	(16^+)	
571.34(4)	21.9(8)	2216.0(5)	1644.6	(18^-)	(16^-)	
573.34(7)	7.7(4)	2892.2(14) [d]	2318.9 [d]			
581.39(5)	8.6(4)	3253.8(6) [d]	2672.4 [d]	(22^-)	(20^-)	
584.90(4)	24.1(8)	3317.5(4)	2732.8	(22^+)	(20^+)	
587.88(6)	11.9(5)	2778.5(4)	2190.8	(19^+)	(17^+)	
602.73(4)	21.8(8)	2525.4(5)	1922.6	(19^-)	(17^-)	
606.88(9)	7.0(4)	2346.2(5) [d]	1738.9 [d]	(19^-)	(17^-)	
608.51(6)	11.3(5)	3087.8(5)	2479.4	(20^+)	(18^+)	
608.75(7)	9.1(5)	2955.0(7) [d]	2346.2 [d]	(21^-)	(19^-)	
612.16(12)	7.9(6)	1059.5(8) [d]	447.3 [d]		(12^-)	
614.20(4)	18.1(7)	3646.6(5)	3032.4	(23^+)	(21^+)	
621.47(8)	5.9(4)	2672.4(6) [d]	2050.9 [d]	(20^-)	(18^-)	
621.95(6)	13.5(7)	2360.7(5) [d]	1738.9 [d]	(19^-)	(17^-)	
624.01(4)	21.2(8)	2050.9(4) [d]	1427.0 [d]	(18^-)	(16^-)	0.92(9)
626.31(7)	7.3(4)	3518.5(15) [d]	2892.2 [d]			
627.70(7)	8.8(4)	3406.5(5)	2778.5	(21^+)	(19^+)	
629.80(6)	8.0(4)	3883.6(7) [d]	3253.8 [d]	(24^-)	(22^-)	
633.15(5)	15.0(6)	2849.1(5)	2216.0	(20^-)	(18^-)	
646.36(9)	6.3(4)	3734.8(7)	3087.8	(22^+)	(20^+)	
647.72(5)	13.3(5)	3965.3(5)	3317.5	(24^+)	(22^+)	
656.36(10)	3.8(3)	3611.3(9) [d]	2955.0 [d]	(23^-)	(21^-)	
663.36(7)	8.6(4)	3188.3(6)	2525.4	(21^-)	(19^-)	
663.51(22)	2.3(3)	4070.0(15)	3406.5	(23^+)	(21^+)	
676.29(8)	7.2(4)	4322.9(7)	3646.6	(25^+)	(23^+)	
678.98(12)	3.4(3)	4413.8(10)	3734.8	(24^+)	(22^+)	

TABLE I. (*Continued*).

E_γ [a] (keV)	I_γ	E_i [b] (keV)	E_f [b] (keV)	$J_i^\pi(\hbar)$	$J_f^\pi(\hbar)$	DCO
679.22(11)	3.8(3)	4197.8(17) [d]	3518.5 [d]			
680.30(8)	4.4(3)	4563.9(9) [d]	3883.6 [d]	(26^-)	(24^-)	
689.74(10)	4.2(4)	3050.4(8) [d]	2360.7 [d]	(21^-)	(19^-)	
692.67(7)	7.8(4)	3541.7(7)	2849.1	(22^-)	(20^-)	
697.14(7)	6.8(4)	2748.1(6) [d]	2050.9 [d]	(20^-)	(18^-)	
707.46(18)	1.9(3)	4318.8(14) [d]	3611.3 [d]	(25^-)	(23^-)	
707.93(7)	7.7(4)	4673.2(7)	3965.3	(26^+)	(24^+)	
716.75(9)	4.8(3)	3767.2(10) [d]	3050.4 [d]	(23^-)	(21^-)	
721.23(8)	6.7(4)	3909.5(9)	3188.3	(23^-)	(21^-)	
730.52(14)	4.1(3)	5294.2(11) [d]	4563.9 [d]	(28^-)	(26^-)	
732.29(13)	2.6(2)	4930.0(19) [d]	4197.8 [d]			
733.65(9)	4.8(3)	3481.7(8) [d]	2748.1 [d]	(22^-)	(20^-)	
737.06(14)	3.8(3)	5059.9(11)	4322.9	(27^+)	(25^+)	
749.25(9)	5.0(3)	4290.9(10)	3541.7	(24^-)	(22^-)	
757.42(19)	1.8(2)	5076.2(18) [d]	4318.8 [d]	(27^-)	(25^-)	
766.74(13)	3.8(3)	5439.9(11)	4673.2	(28^+)	(26^+)	
776.71(14)	3.4(3)	4686.3(14)	3909.5	(25^-)	(23^-)	
785.42(29)	1.2(2)	5715.5(26) [d]	4930.0 [d]			
796.38(24)	1.9(2)	5856.3(19)	5059.9	(29^+)	(27^+)	
798.60(16)	2.7(3)	5089.6(16)	4290.9	(26^-)	(24^-)	
819.72(34)	1.1(2)	5505.7(23)	4686.3	(27^-)	(25^-)	
823.67(22)	2.1(2)	6263.6(17)	5439.9	(30^+)	(28^+)	
845.00(38)	0.4(2)	5934.6(31)	5089.6	(28^-)	(26^-)	
853.68(100)	0.1(2)	6710.0(0)	5856.3	(31^+)	(29^+)	
876.62(40)		7140.2(30)	6263.6	(32^+)	(30^+)	
883.00(22)		6817.6(35)	5934.6	(30^-)	(28^-)	

[a]Uncertainties in parentheses are statistical only. Systematic uncertainty is 0.2 keV.
[b]Energies relative to the (7^+) head of band 6.
[c]Transitions placed below the (8^-) level of band 9.
[d]Energies relative to the (8^-) level of band 9.
[e]Combined DCO of 140.97 and 141.87 keV transitions.

shows lines associated with bands 7–10. Band 7 is linked tentatively to band 9 via a 479 keV transition. Ambiguities arise due to a 462 keV line (not placed on the level scheme), which lies close in energy to the 460 keV transition in band 7, and which is in coincidence with the 479 keV line and members of band 9 below the (12^-) level. Band 8 is only linked to band 9 via the 621 keV transition, although other paths linking the bands together must exist, since the 423, 475, and 516 keV transitions are in coincidence with transitions placed near the head of band 9 [cf. Fig. 2(c)]. Furthermore, the lowest four transitions of band 8 are in coincidence with the 97 keV transition that is placed below band 1. Again, the path by which intensity reaches the 97 keV transition could not be determined. The present data for band 9 disagrees with Zhang *et al.* [13] at high spins. A 705 keV transition, placed as the $(21^-)\rightarrow(19^-)$ in Ref. [13], was not observed in this work. Instead, transitions of 690 and 717 keV are placed in the band. Five lines, of 53.0, 55.5, 56.8, 61.5, and 69.4 keV energy, are in mutual coincidence and also in coincidence with transitions placed in band 9. They are clearly visible in the low energy photon (LEP) spectrum shown in Fig. 4, formed by summing gates on transitions in band 9. The theoretical total conversion coefficients for $E1$, $M1$, and $E2$ transitions of energies below 70 keV differ by orders of magnitude. For instance, at 56.8 keV, they are 0.37, 5.89, and 58.8, respectively. If it is assumed that these five transitions depopulate the (8^-) level of band 9 in a cascade, their multipolarities can be deduced from the 296 $+435$ keV coincidence gate by balancing their intensity with the sum of the 131 and 152 keV transition intensities. Predominantly $M1$ multipolarity is indicated, suggesting that these lines may be transitions between low-spin levels of the band. However, they are not shown in the level scheme, but are listed in Table I, because their ordering and therefore placement could not be determined.

IV. DISCUSSION

A. Expected configurations

We first note that the one-quasiparticle configurations known to be nearest to the Fermi surface in the odd neighbors [17,24,25] are the neutron orbitals $\nu 5/2^-[512]$, $\nu 1/2^-[521]$, and $\nu 7/2^+[633]$ and proton orbit-

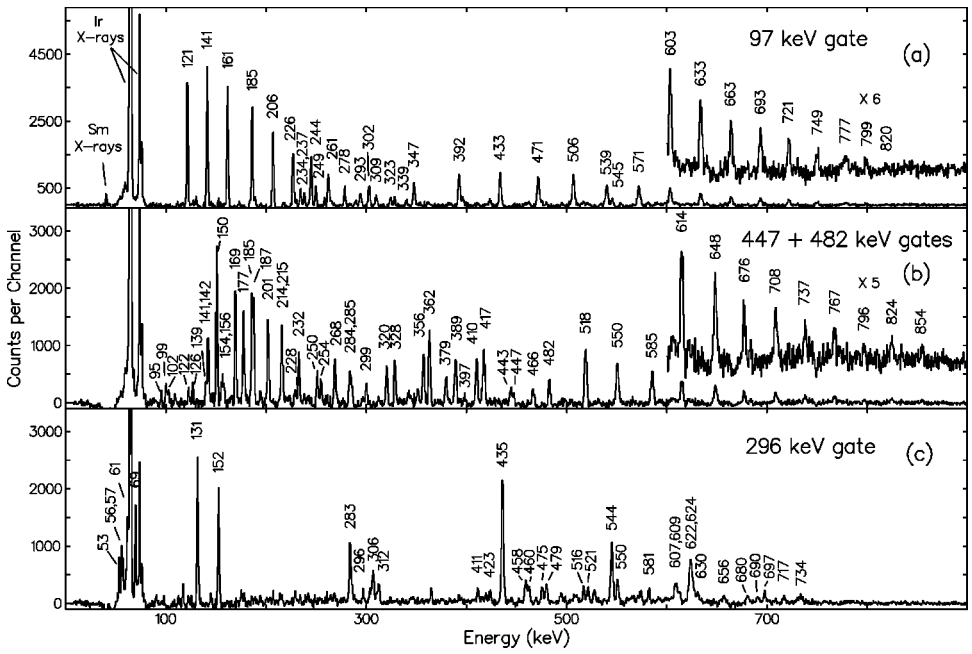

FIG. 2. Coincidence spectra obtained by gating on (a) the 97 keV line, (b) the 482 and 447 keV lines, and (c) the 296 keV line.

als based on the $\pi h_{9/2}$, $\pi d_{5/2}$, $\pi d_{3/2}$, and $\pi h_{11/2}$ configurations. Slightly further from the Fermi surface lie the $\pi f_{7/2}$ and $\pi i_{13/2}$ orbitals. Two-quasiparticle configurations formed by coupling the proton and neutron orbitals together are listed in Table II, along with an estimate of aligned angular momenta and bandhead energies, based on averages obtained from observed one-quasiparticle bands in the neighboring nuclei. The estimates of bandhead energies are for the high-K coupling only, and do not include contributions from the Coriolis interaction, which may also compress the levels near the bandhead and lead to a higher bandhead spin, nor do they include Gallagher-Moszkowski splitting [26]. The energy estimates must also be tempered by the knowledge that the light Ir isotopes lie in a region of softness. Thus deformation changes will also influence bandhead energies.

To assign configurations to the observed bands, we consider the observed properties of the bands including alignments, band crossings, and ratios of transition rates.

Aligned angular momenta for the bands in ^{176}Ir are plotted in Fig. 5, using a reference which gives a relatively constant aligned angular momentum for the $\pi h_{9/2} \otimes \nu i_{13/2}$ band. For comparison, alignments of neighboring nuclei are shown in Fig. 6. The presence of alignment can also be deduced from the plots of energy vs spin, shown in Fig. 7. Because the energy of an aligned band is given by $E \simeq E_0 + A(I-i) \times (I-i+1)$, the alignment i would normally shift the minimum of energy to spin $I_{min} = i - 1/2$, but since a rigid rotor has been subtracted in Fig. 7, the relationship is modified to $I_{min} \simeq 2i$.

Experimental values of $B(M1)/B(E2)$ for are shown in Figs. 8 and 9. These were obtained by estimating the square

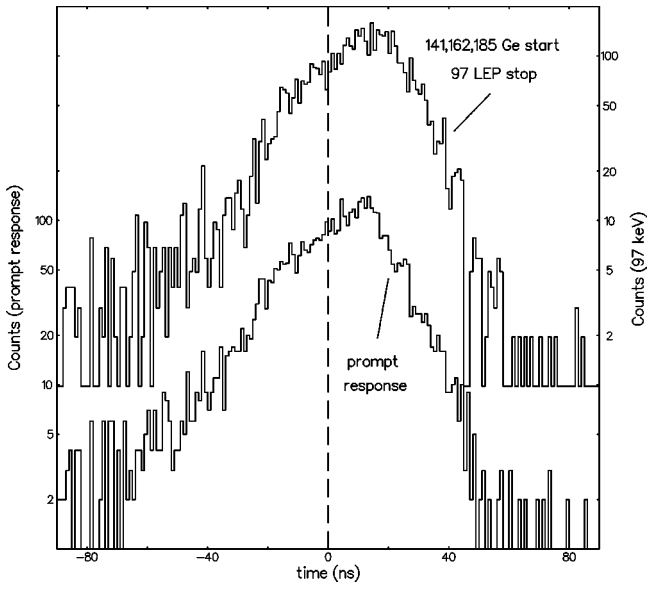

FIG. 3. Time difference spectrum constructed with gates on transitions of band 1, detected in the Ge detectors as ''start,'' and the 97 keV γ ray detected in the LEPS detectors as ''stop,'' compared to the prompt response function for the corresponding energies. Time dispersion is 1 ns per channel.

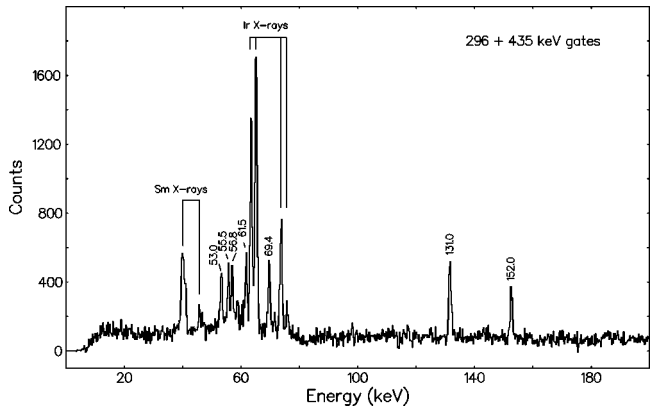

FIG. 4. LEP spectrum formed by summing the 296 and 435 keV coincidence gates on the recoil-into-vacuum data.

TABLE II. Zero order level scheme for ^{176}Ir.

	$\pi 1/2^-[541]\downarrow$	$\pi 9/2^-[514]\uparrow$	$\pi 5/2^+[402]\uparrow$	$\pi 3/2^+[402]\downarrow$	$\pi 1/2^-[530]\uparrow$	$\pi 1/2^+[660]\uparrow$
E [a]	0 keV	~100 keV	117 keV	~150 keV	~350 keV	733 keV
i_x [b]	$3\hbar$	$0\hbar$	$0\hbar$	$0\hbar$	$2.5\hbar$	$6\hbar$
$\nu 5/2^-[512]\uparrow$	3^+	7^+	5^-	4^-	3^+	3^-
0 keV	0 keV	~100 keV	117 keV	~150 keV	~350 keV	733 keV
$0\hbar$	$3\hbar$	$0\hbar$	$0\hbar$	$0\hbar$	$2.5\hbar$	$6\hbar$
$\nu 7/2^+[633]\uparrow$	4^-	8^-	6^+	5^+	4^-	4^+
100 keV	100 keV	~200 keV	217 keV	~250 keV	~450 keV	833 keV
$3\hbar$	$6\hbar$	$3\hbar$	$3\hbar$	$3\hbar$	$5.5\hbar$	$9\hbar$
$\nu 1/2^-[521]\downarrow$	1^+	5^+	3^-	2^-	1^+	1^-
125 keV	125 keV	~225 keV	242 keV	~275 keV	~475 keV	858 keV
$1\hbar$	$4\hbar$	$1\hbar$	$1\hbar$	$1\hbar$	$3.5\hbar$	$7\hbar$

[a]Proton and neutron energies, averages of neighboring nuclei.
[b]Aligned angular momenta.

of the mixing ratio, δ^2, with the rotational model, using the K value of the proposed configuration. Such values of δ^2 were all less than 0.3, so a misassigned K value will introduce an error of less than 30%.

The experimental values are compared with values calculated using the semiclassical expression for the $B(M1)$ values [28]:

$$B(M1,I\rightarrow I-1)=\frac{3}{8\pi I^2}\left\{\sqrt{I^2-K^2}\left[\sum_j (g_j-g_R)\Omega_j\right]-K\left[\sum_j (g_j-g_R)i_j\right]\right\}^2 \mu_N^2. \quad (1)$$

The collective g factor g_R was fixed at Z/A while other g factors, listed in Ref. [14], were estimated from the wave functions of Chi [29]. The one-quasiparticle alignments i were taken as $3\hbar$ for the $\pi h_{9/2}$ and $\nu i_{13/2}$ orbitals and $6\hbar$ for the $\pi i_{13/2}$ orbital as seen in Fig. 6. Omega values were fixed at the values of the corresponding Nilsson orbital, except for the $\nu i_{13/2}$ orbital, and Ω was fixed at $3\hbar$ to approximately account for Coriolis mixing.

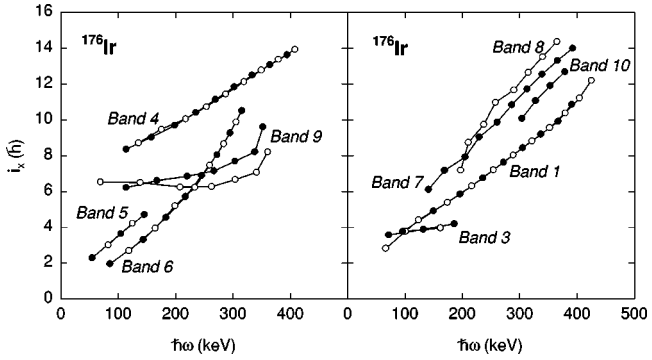

FIG. 5. Aligned angular momenta for bands in ^{176}Ir. Reference parameters: $J_0=30$ MeV$^{-1}\hbar^2$, $J_1=45$ MeV$^{-3}\hbar^4$.

A further test of configuration is provided by the sign of δ, which, for prolate systems, should equal the sign of g_K-g_R. In the presence of alignment the strong coupling formula for g_K-g_R should be replaced by one for an effective g_K, or g_{eff} since in general g_{eff} is spin dependent:

$$g_{eff}-g_R=\frac{\Sigma(g_j-g_R)K_j}{K}-\frac{\Sigma(g_j-g_R)i_j}{\sqrt{I^2-K^2}}. \quad (2)$$

Table III lists average DCO ratios for sufficiently intensely populated bands, from which the sign of the mixing ratio is deduced. These are compared with average values of g_{eff} for the configurations proposed in Sec. IV C.

To calculate the $B(E2)$ values, quadrupole moments, obtained from calculations outlined in the next section, were

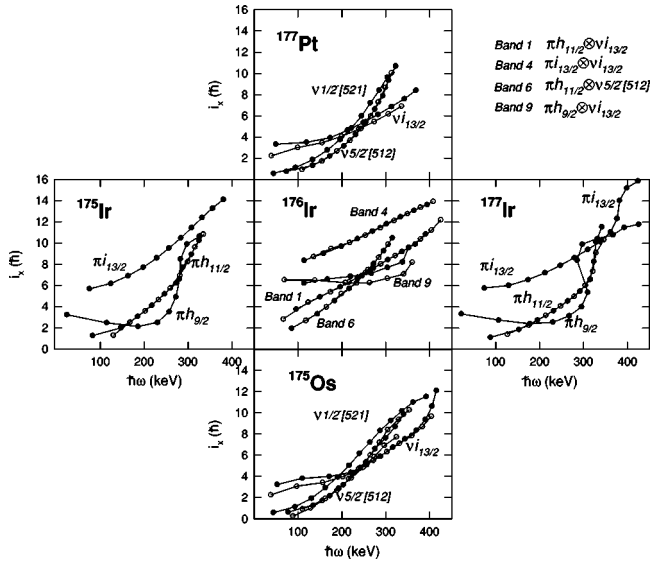

FIG. 6. Aligned angular momenta for selected bands in ^{176}Ir compared to those of neighboring nuclei. Reference parameters are as in Fig. 5. Data are from Refs. [17,24,25,27].

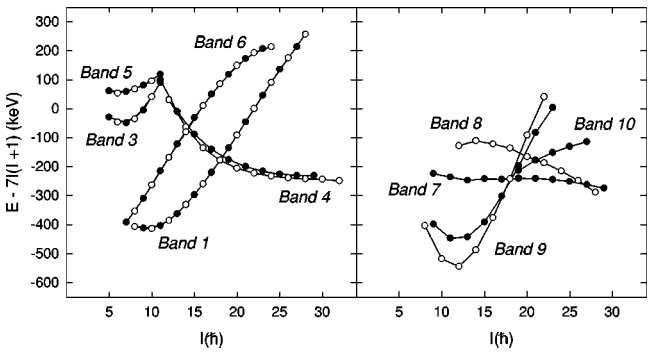

FIG. 7. Energy vs spin for bands in ^{176}Ir. A rigid-rotor reference has been subtracted.

employed. Like the bandhead energies, the nuclear deformation is expected to be configuration dependent.

B. Configuration dependent deformations

We consider the likely shapes to be encountered in ^{176}Ir by beginning with an overview of the shapes encountered in the neighboring nuclei. In the even-even Pt isotopes, evidence is accumulating for a ground band perturbed by mixing between weakly deformed triaxial and well-deformed prolate structures, in a manner reminiscent of the prolate-oblate shape coexistence known in the Hg isotopes. Indeed, a well-defined band crossing occurs near spin $4\hbar$ in the nearby nucleus ^{176}Pt [30–32]. Analogous band crossings have been observed in the $\pi h_{11/2}$ bands of the lightest odd-Z Ir isotopes, $^{171-173}$Ir [33,34]. In these isotopes, although no firm spin assignments have been made for these bands, it is proposed that a triaxial $\pi h_{11/2}$ band, based on an $11/2^-$ state, is crossed by a prolate $\pi h_{11/2}$ band based on a $9/2^-$, $(9/2^-[514])$ state. In ^{175}Ir and heavier isotopes, the $9/2^-$ band is proposed to lie lower than the $11/2^-$ band and so the crossing no longer occurs [17,34,35], but evidence of mixing persists in the form of a depressed first excited state of the $9/2^-$ band, taken to have a spin of 11/2. Thus in ^{176}Ir the

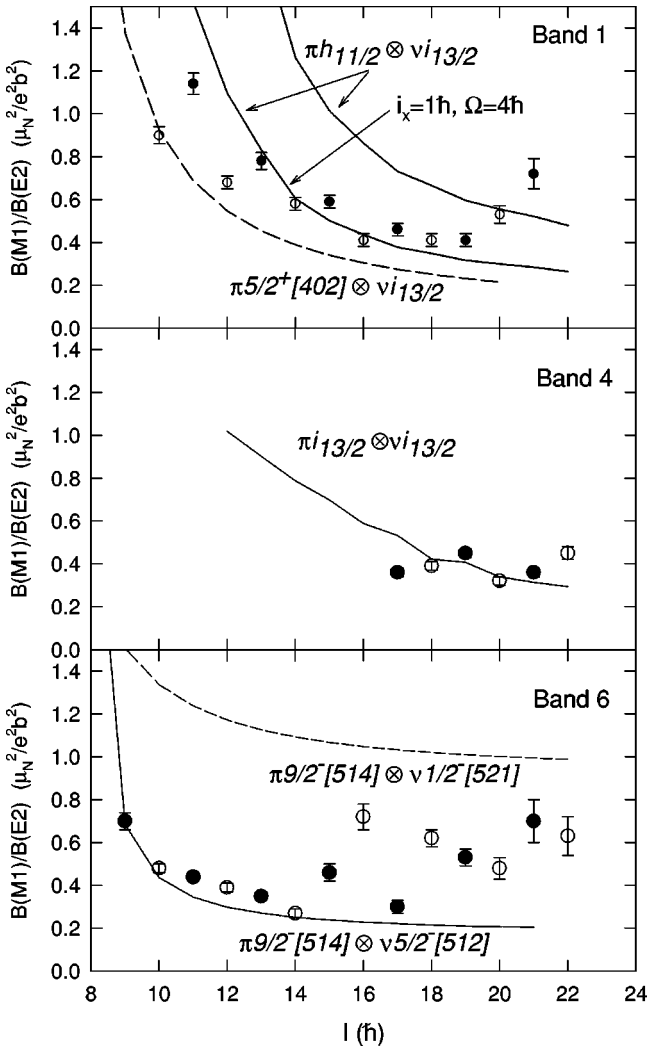

FIG. 8. Comparison of theoretical and experimental $B(M1)/B(E2)$ values for bands 1, 4, and 6.

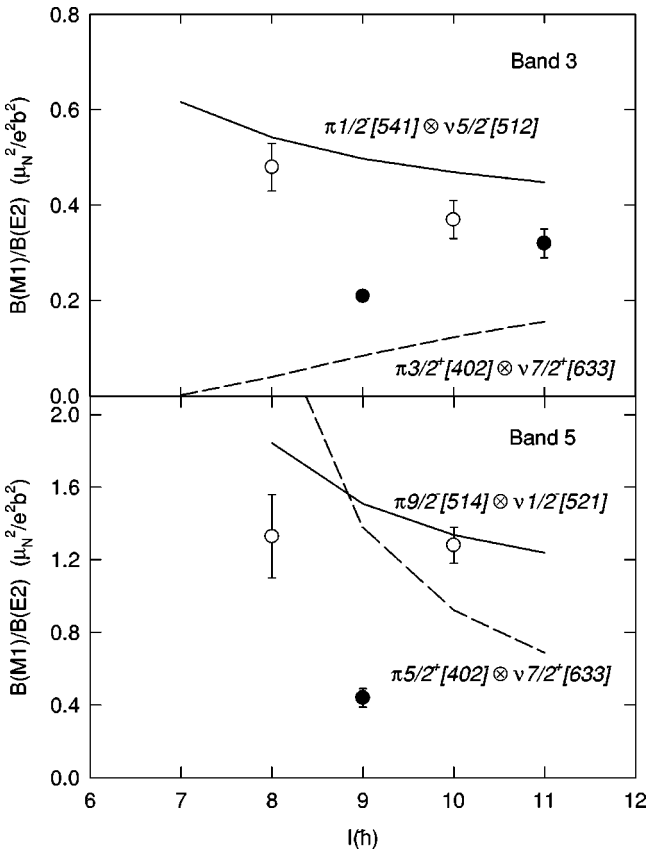

FIG. 9. Comparison of theoretical and experimental $B(M1)/B(E2)$ values for bands 3 and 5.

TABLE III. Comparison of average DCO ratios, sign $\delta_{\rm exp}$, and theoretical $g_{eff}-g_R$ values.

Band	⟨DCO⟩	Sign $\delta_{\rm exp}$	$(g_{eff}-g_R)_{\rm th}$	Configuration
1	0.68(7)	~ 0	1.0	$\pi h_{11/2}\otimes \nu i_{13/2}$
4	0.38(6)	<0	-0.7	$\pi i_{13/2}\otimes \nu i_{13/2}$
6	0.90(6)	>0	0.4	$\pi h_{11/2}\otimes \nu 5/2^-[512]$
9	0.38(5)	<0	-0.3	$\pi h_{9/2}\otimes \nu i_{13/2}$

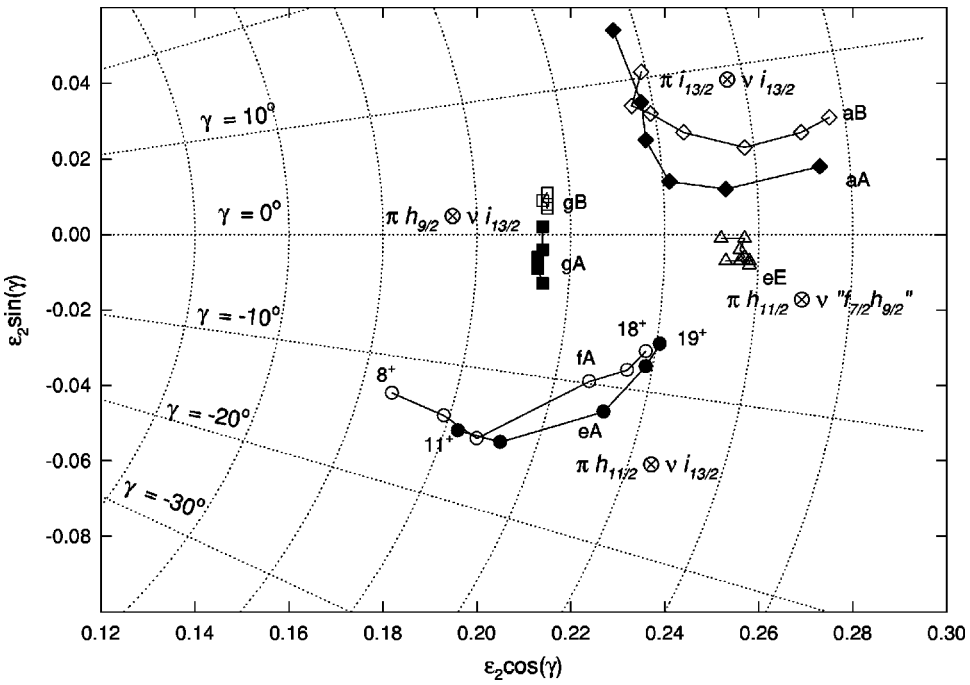

FIG. 10. Calculated deformations for configurations in ^{176}Ir. Letter labels: A, B—$\nu i_{13/2}$, $\alpha = +\frac{1}{2}, -\frac{1}{2}$; E—$\nu f_{7/2}h_{9/2}$, $\alpha = +\frac{1}{2}$; e, f—$\pi h_{11/2}, \alpha = +\frac{1}{2}, -\frac{1}{2}$; g—$\pi h_{9/2}, \alpha = +\frac{1}{2}$; a—$\pi i_{13/2}, \alpha = +\frac{1}{2}$.

Fermi surface is taken to lie closer to the $\Omega = 9/2$ orbital than the $\Omega = 11/2$ orbital at prolate deformation in the $\pi h_{11/2}$ subshell. Furthermore, the $B(M1)/B(E2)$ values of the $\pi h_{11/2}$ bands of $^{175-181}$Ir have systematically low values, which has been described by a band-mixing model where a $\pi h_{11/2}$ band of low deformation mixes with one of larger deformation, giving rise to $B(E2)$ values increasing with spin, and therefore to lower $B(M1)/B(E2)$ values [17,36,37]. The aligned angular momenta of the $\pi h_{11/2}$ bands, compared to those of the $\pi h_{9/2}$ bands, support either this scenario, or one in which the $\pi h_{11/2}$ bands are more deformed than the $\pi h_{9/2}$ bands. They increase gradually, when a reference is chosen that keeps the alignment of the $\pi h_{9/2}$ bands constant, implying a larger moment of inertia. Although differences emerge in the details depending on the choice of potential, these conclusions are broadly supported by potential energy surface calculations based either on the Woods-Saxon or harmonic oscillator potentials [18,34,38–40]. For example, in ^{175}Ir, TRS calculations predict a constant deformation of $\beta_2 = 0.22$ for the $\pi h_{9/2}$ band, while predictions of β_2 increase from 0.17 to 0.25 before the alignment of $i_{13/2}$ neutrons [18] for the $\pi h_{11/2}$ band. However, near $N = 98$, the situation is complicated by the strong interactions predicted by the cranked shell model [41] at the crossing with the *S* band, formed by the alignment of $i_{13/2}$ neutrons. This is expected to contribute significantly to the gradual upbending of the aligned angular momenta of the bands shown in Fig. 6.

To understand the expected shapes in the doubly odd nucleus ^{176}Ir, one must also take account of the shape driving properties of the odd neutron. An $i_{13/2}$ neutron, for example, could be expected to drive towards negative values of the triaxiality parameter γ and smaller values of ε_2 [42]. Therefore, to account for competing polarization tendencies, potential energy surface calculations were carried out using the Nilsson-Strutinsky code "ULTIMATE CRANKER" [43,44], using the parameter set of Zhang *et al.* [45], which is optimized for the Pt region. Similar calculations for the odd-proton Ir isotopes were carried out recently in Ref. [34], where a comparison of the results using the parameters of Zhang *et al.* [45] and the standard parameters [46] is made. Predicted deformations, as a function of spin, for low-lying configurations formed by coupling an $i_{13/2}$ neutron to either an $h_{9/2}$, $h_{11/2}$, or $i_{13/2}$ proton, are plotted in Fig. 10. The $\pi h_{11/2} \otimes \nu i_{13/2}$ and $\pi h_{9/2} \otimes \nu i_{13/2}$ bands are predicted to mimic the proposed shape evolution of the corresponding $\pi h_{9/2}$ and $\pi h_{11/2}$ bands in the odd-*Z* Ir isotopes: the $\pi h_{11/2} \otimes \nu i_{13/2}$ band is predicted to be triaxial and increase (or stretch) in quadrupole deformation as a function of spin, while the $\pi h_{9/2} \otimes \nu i_{13/2}$ band is calculated to have a relatively stable deformation. Also predicted to stretch is the $\pi i_{13/2} \otimes \nu i_{13/2}$ band, which mimics the predicted shape evolution of the one-quasiparticle $\pi i_{13/2}$ band [27,38]. Calculations were also performed for couplings to negative-parity neutrons. For example, the $\pi h_{11/2} \otimes \nu 5/2^-[512]$ and $\pi h_{11/2} \otimes \nu 1/2^-[521]$ configurations were predicted to have stable prolate deformations with ε_2 between 0.25 and 0.26.

C. Configuration and spin assignments

1. Band 4 — $\pi i_{13/2} \otimes \nu i_{13/2}$ band

Due to the loss of intensity to bands 3, 5, and 6, it is likely that the head of band 4 has not been observed, but the lowest state observed puts an upper limit of approximately 1000 keV on its bandhead. Such an excitation energy is too low for a four-quasiparticle band, which would be expected to lie closer to $2\Delta \simeq 2000$ keV. The strong population of the band is consistent with it being yrast at high spins, implying a band with a large aligned angular momentum, and it is thus a prime candidate for the $\pi i_{13/2} \otimes \nu i_{13/2}$ band. This assignment [47] is supported by the good agreement found for the $B(M1)/B(E2)$ values, as shown in Fig. 8, and the sign of the mixing ratio, listed in Table III. With the present spin

assignments to the band, which follow from the assignments made to band 6 in the next section, the aligned angular momentum of the band near $\hbar\omega=250$ keV, $9\hbar$, is in good agreement with the alignment expected for the proposed configuration. The gradual upbending is likely to be due partly to the choice of reference, which flattens the alignment curve of band 8, and due to the predicted increase in deformation. It is qualitatively consistent with a large moment of inertia associated with the $\pi i_{13/2}\otimes\nu i_{13/2}$ band.

2. Band 6 — $\pi 9/2^-[514]\otimes\nu 5/2^-[512]$ band

The parity of band 6 is positive, as implied by the transitions which link it to band 4, presumed to be due to mixing of the nearly degenerate (14^+) states. Furthermore, at low frequency, it has the lowest aligned angular momentum of any of the observed bands, close to $2\hbar$. This rules out any configurations involving $h_{9/2}$, $f_{7/2}$, and $i_{13/2}$ protons, or the $i_{13/2}$ neutron. Thus an $h_{11/2}$ proton must be coupled to a negative-parity neutron. Following the discussion in Sec. IV B, the proton Fermi surface is taken to lie closer to the $\Omega=9/2$ orbital of the $h_{11/2}$ subshell, rather than the $\Omega=11/2$ orbital, giving two low-lying configurations as candi dates, the $\pi 9/2^-[514]\otimes\nu 1/2^-[521]$ and $\pi 9/2^-[514]\otimes\nu 5/2^-[512]$ configurations. While both would have positive mixing ratios, the latter is in good agreement with the measured $B(M1)/B(E2)$ values while the former overestimates the values by up to a factor of 5. Thus $K^\pi=7^+$ is assigned [47] to the bandhead, thereby also fixing the spins of band 4. The rise in the experimental $B(M1)/B(E2)$ values above spin 14 is qualitatively consistent with a gradual alignment of $i_{13/2}$ neutrons, although no correction has been made in the data for mixing with band 4 at spin 14.

3. Bands 3 and 5

Bands 3 and 5 are linked to band 4, presumably due to the mixing of levels near spins 11 and 12, and are thus assigned positive parity. Due to the low intensity and low energy transitions, identification of their bandheads is uncertain, but upper limits of 5^+ and 6^+, respectively, are placed on their spins. Comparison of experimental $B(M1)/B(E2)$ ratios with theoretical ratios of candidate configurations is made in Fig. 9. The increase of the $B(M1)/B(E2)$ values of band 3 at low spins favors a tentative $\pi 1/2^-[541]\otimes\nu 5/2^-[512]$ assignment, which is consistent with the observed aligned angular momentum. For band 5, the $B(M1)/B(E2)$ values are inconclusive, but the alignment pattern favors a tentative $\pi 9/2^-[514]\otimes\nu 1/2^-[521]$ assignment: Band 5 has approximately $1\hbar$ more aligned angular momentum than band 6, corresponding to the replacement of the $5/2^-[512]$ neutron by a $1/2^-[521]$ neutron.

4. Band 1 — $\pi 9/2^-[514]\otimes\nu 7/2^+[633]$ band

Band 1, a strongly coupled structure populated to high excitation energy, presumably lies close to the yrast line. Two configurations, $\pi 9/2^-[514]\otimes\nu 7/2^+[633]K^\pi=8^-$ and $\pi 5/2^+[402]\otimes\nu 7/2^+[633]K^\pi=6^+$, are candidates for this band. The former would be expected to lie closest to the yrast line due to its higher-K value. Indeed, in the odd-proton Ir isotopes, the $\pi 9/2^-[514]$ band is populated more strongly and to higher spin than the $\pi 5/2^+[402]$ band [17,40]. However, as shown in Fig. 8, the $B(M1)/B(E2)$ values fit the $K^\pi=6^+$ calculation better. The problem with a $K^\pi=6^+$ assignment is that the nonobservation of the $K^\pi=8^-$ band would need to be explained. In the odd-proton isotopes, the $B(M1)/B(E2)$ values of the $\pi 9/2^-[514]$ band are consistently low unless a relatively large deformation, $Q_t=8.0e$ b, is assumed in the calculation. In ^{176}Ir, the calculated $B(M1)/B(E2)$ values, using transition quadrupole moments corresponding to the predicted deformations, which reach a maximum of 7.3 e b by spin 19, are still overestimated. Surprisingly, Zhang *et al.* [47] found good agreement between calculated and measured $B(M1)/B(E2)$ values in ^{178}Ir by ignoring alignment and assuming only the strong coupling expression for the g_K value.

However, good agreement can also be found if it is assumed that the $9/2^-[514]$ proton is slightly Fermi aligned, (justified if indeed the band is associated with the predicted triaxial shape), with $\Omega=4\hbar$ and $i_x=1\hbar$, as shown in Fig. 8. Band 1 is therefore assigned to the $K^\pi=8^-$, $\pi 9/2^-[514]\otimes\nu 7/2^+[633]$ configuration, in agreement with Ref. [13].

It is interesting to note that the relative size of the splitting in $B(M1)/B(E2)$ values (Fig. 8) has no correspondence in the energy signature splitting of the band. Such a mismatch is also possible evidence of triaxiality [48].

If $K^\pi=8^-$ is assigned to the head of band 1, the 97 keV $E1$ transition depopulating the band could be a decay to the head of band 6, which is the only available intrinsic state with $K^\pi=7^+$ (see Table II). Its 4.1 nsec mean life would then correspond to a $B(E1)$ value of $5.75(70)\times10^{-5}$ W.u. for a $\nu 7/2^+[633]\rightarrow\nu 5/2^-[512]$ transition. This is slightly higher than the strengths reported for this transition at $N=99$ in the literature [49], which are typically below 3×10^{-5} W.u.

5. Band 9 — $\pi h_{9/2}\otimes\nu i_{13/2}$ band and bands 7, 8, and 10

Band 8 is assigned [13] to the $\pi h_{9/2}\otimes\nu i_{13/2}$ configuration, which is similar in structure to those reported in heavier Ir isotopes [47]. A negative mixing ratio is found for this band as expected. The spins were estimated by using additivity of aligned angular momentum, and by requiring a signature inversion at low spin, as observed for this band in other nuclei [7–10].

In the odd-proton Ir isotopes, the favored signature of the $\pi h_{9/2}$ band is fed by its unfavored signature, and also by the $\pi f_{7/2}$ band [17,18,40]. Bands 7, 8, and 10 feed into band 9, and it is therefore natural to think of these as being candidates for structures formed by coupling an $i_{13/2}$ neutron to the corresponding bands of the odd-Z neighbors. Another possibility, since the multipolarities of the linking transitions are unknown, is the doubly decoupled $\pi 1/2^-[541]\otimes\nu 1/2^-[521]$ band. However, inspection of Fig. 7 reveals that the situation is likely to be more complicated. Bands 7 and 8 have an irregular dependence on energy, which could indicate crossings with other bands whose levels could not be observed due to low or fragmented intensity. Certainly, at the highest frequencies, the bands reach alignments of up to

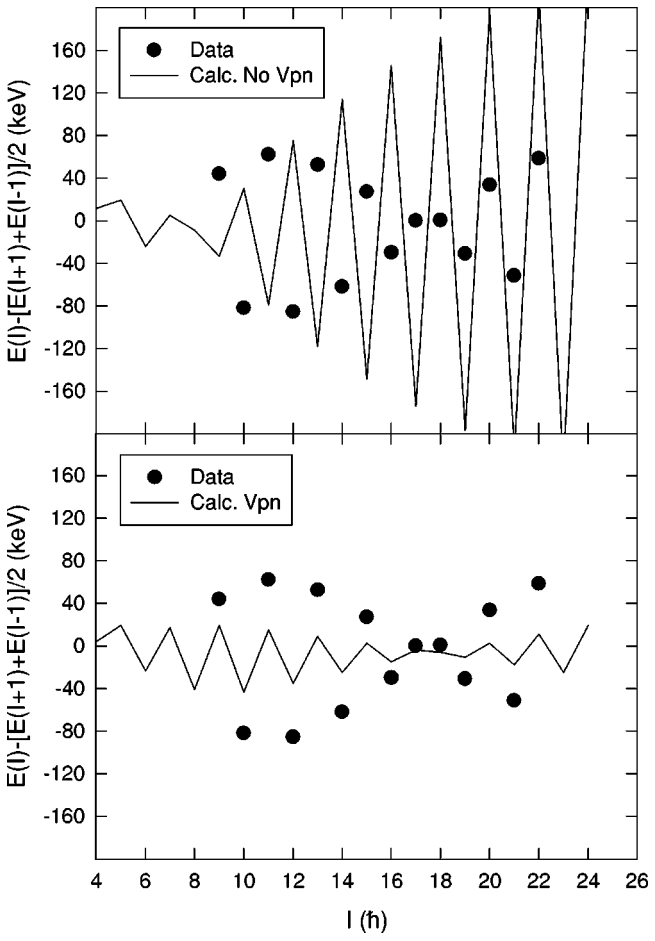

FIG. 11. Staggering in the $\pi h_{9/2} \otimes \nu i_{13/2}$ band compared with predictions of the particle-rotor model with and without the residual interaction V_{pn}.

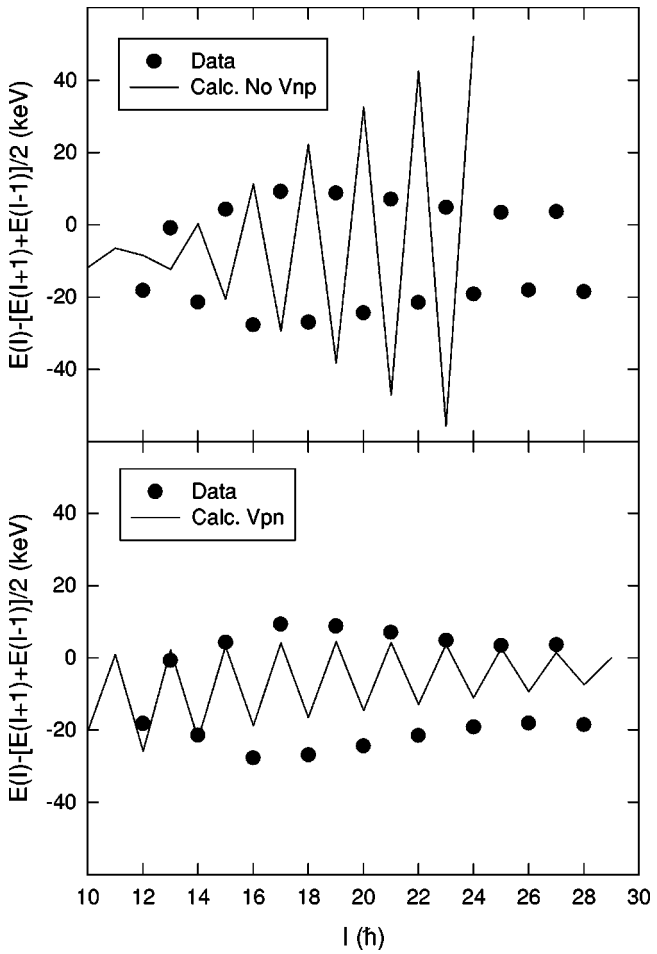

FIG. 12. Staggering in the $\pi i_{13/2} \otimes \nu i_{13/2}$ band compared with predictions of the particle-rotor model with and without the residual interaction V_{pn}.

$14\hbar$, which would imply four-quasiparticle character, presumably due to the alignment of further $i_{13/2}$ neutrons.

D. Residual interactions and signature inversion

The bands which show substantial signature splitting, in which both signature branches have been observed, are bands 4 and 9, which are assigned to the $\pi h_{9/2} \otimes \nu i_{13/2}$ and $\nu i_{13/2} \otimes \nu i_{13/2}$ configurations. These are both expected to have the signature $\alpha = 1$ favored by the Coriolis interaction. However, with the present spin assignments, this is not the case experimentally. The signature splitting of the bands is demonstrated in the staggering plots of Figs. 11 and 12, in which the favored signature lies lowest.

Although firm spins could not be assigned to the $\pi h_{9/2} \otimes \nu i_{13/2}$ band, it is nevertheless clear from the staggering plot in Fig. 11 that a change in phase in the signature splitting occurs near spin 17. Thus a signature inversion occurs in at least a spin interval either above or below spin 17. Note that this change in phase cannot be attributed to a band crossing in one signature partner and not the other, since a crossing is only evident in the alignment curve (Fig. 6), at the highest of spins (near 350 keV), and occurs in both branches. In contrast, with the present spin assignments, the $\pi i_{13/2} \otimes \nu i_{13/2}$ band is inverted over the entire observed spin range (Fig. 12).

To account for these inversions, we employ the particle-rotor model, specifically, the code of Semmes and Ragnarsson [3,4], to test whether these signature splitting effects could be accounted for by the standard particle-rotor model or whether they could be explained by the inclusion of a residual interaction. In these calculations, a variable moment of inertia [50] was used to describe the behavior of the core. Since the occupation of the $h_{9/2}$ proton orbital results in a substantially different moment of inertia to the remaining bands (cf. Fig. 6), different moment of inertia parameters were employed for the two bands. The moment of inertia of the $\pi h_{9/2} \otimes \nu i_{13/2}$ band was obtained from a fit to the $h_{9/2}$ band of ^{177}Ir, while the moment of inertia for the $\pi i_{13/2} \otimes \nu i_{13/2}$ band was obtained from a fit to the ground band of ^{174}Os. In both calculations the Coriolis interaction was attenuated by a factor of 0.8.

The calculations were performed both with, and without, a residual proton-neutron interaction having the form

$$V_{pn} = \sqrt{8\pi^3}\left(\frac{\hbar}{m\omega}\right)^{3/2} \delta(\mathbf{r}_p - \mathbf{r}_n)(u_0 + u_1 \sigma_p \cdot \sigma_n). \quad (3)$$

The values of the parameters u_0 and u_1 were fixed at -4.95 MeV and -0.55 MeV, respectively, which are optimized for the rare-earth region [10]. The standard Nilsson parameters of Bengtsson and Ragnarsson [46] were used.

1. $\pi h_{9/2} \otimes \nu i_{13/2}$ band

To calculate the $\pi h_{9/2} \otimes \nu i_{13/2}$ band, the orbitals selected for the Coriolis diagonalization included all those from the neutron $i_{13/2}$ subshell, and as in Refs. [7,8], the low Ω orbitals from the proton $f_{7/2}$ and $h_{9/2}$ subshells, $\Omega = 1/2,3/2$ and 1/2, 3/2, 5/2, and 7/2, respectively. The deformation $(\varepsilon_2, \gamma) = (0.21,0)$ was chosen to be consistent with the calculated values.

The results are compared with experiment on the staggering plots of Fig. 11. The calculations without V_{pn} predict a change in phase of the staggering at low spin, but clearly it does not reproduce the observed change in phase near spin 17. The predicted phase change is due to an angular momentum recoupling for $I < j_\pi + j_\nu$, as discussed, e.g., by Hamamoto [1]. The inclusion of V_{pn}, however, reproduces the observed phase change near spin 17 rather well. Although firm spins have not been assigned to the band, the observation of the high-spin phase change argues strongly for the necessity of including residual proton-neutron interactions, as observed in the lighter, rare-earth nuclei. No attempt has been made to optimize the amplitude of the calculated staggering, but this also depends on other parameters such as the moment of inertia and Coriolis attenuation.

2. $\pi i_{13/2} \otimes \nu i_{13/2}$ band

The Coriolis diagonalization for the $\pi i_{13/2} \otimes \nu i_{13/2}$ band included all orbitals in both $i_{13/2}$ subshells at a deformation of $(\varepsilon_2, \gamma) = (0.25,0)$. The results are shown in Fig. 12. Essentially, neither calculation predicts a change in phase above spin 12. But the calculations are opposite in phase, with the calculations including V_{pn} giving agreement with the data. Furthermore, the calculations with V_{pn} are of nearly constant amplitude, also in agreement with the data, whereas without V_{pn} the amplitude is predicted to increase.

It should be remembered that the present spin assignments can be regarded as reasonably firm, since they depend only on the assumption that the proton Fermi level for the $\pi 9/2^-[514] \otimes \nu 5/2^-[512]$ band lies nearest the $9/2^-[514]$ orbital at a prolate shape, a fact which is supported by the systematic evidence discussed in Sec. IV B.

It is also interesting to note that in odd-proton nuclei, the alignment of $i_{13/2}$ neutrons, when coupled to an $h_{9/2}$ proton, is delayed to a higher rotational frequency compared to the value found in the even-even neighbors of the odd-proton nucleus (see, e.g., Ref. [52]). It has been shown on a phenomenological level that the $\pi h_{9/2} - \nu i_{13/2}$ interaction can account for the increase in crossing frequency [8–10]. It follows that if the p-n interaction is responsible for the signature inversion of $\pi i_{13/2} \otimes \nu i_{13/2}$ bands, a delay in the alignment of $i_{13/2}$ neutrons should also be expected in the $\pi i_{13/2}$ bands. Indeed, in the cases where the band crossing has been unambigously observed in Re and Ir nuclei, a delayed backbending is reported [14,51].

V. CONCLUSION

It is clear from the present observations that in general the signature splitting of a band in doubly odd nuclei cannot be predicted from the properties of the Coriolis force alone. In the model, which includes a residual proton-neutron interaction, the qualitative understanding of the occurrence of signature inversion — that it occurs when a particle is coupled to a quasiparticle — has been borne out by the present observations.

However, it is also clear that further experimental work is necessary, particularly for the $\pi i_{13/2} \otimes \nu i_{13/2}$ band, both to provide firm spin assignments and to map the systematic behavior of the signature splitting as a function of proton and neutron numbers.

ACKNOWLEDGMENTS

We would like to thank the academic and technical staff of the Australian National University Heavy Ion Facility for their continuing support in these studies.

[1] I. Hamamoto, Phys. Lett. B **235**, 221 (1990).
[2] R. Bengtsson, J.A. Pinston, D. Barneoud, E. Monnand, and F. Schussler, Nucl. Phys. **A389**, 158 (1982)
[3] P.B. Semmes and I. Ragnarsson, in *Proceedings of the International Conference on High-Spin Physics and Gamma-Soft Nuclei, Pittsburgh, 1990*, edited by J.X. Saladin, R.A. Sorenson, and C.M. Vincent (World Scientific, Singapore, 1991), p. 500.
[4] Paul B. Semmes and Ingemar Ragnarsson, in *Future Directions in Nuclear Physics with 4π* Gamma Detection Systems of the New Generation, edited by J. Dudek and B. Haas, AIP Conf. Proc. No. 259 (AIP, New York, 1992), p. 566.
[5] Alpana Goel and Ashok K. Jain, Nucl. Phys. **A620**, 265 (1997).
[6] F.R. Xu, W. Satula, and R. Wyss, Nucl. Phys. **A669**, 119 (2000).
[7] R.A. Bark, J.M. Espino, W. Reviol, P.B. Semmes, H. Carlsson, I.G. Bearden, G.B. Hagemann, H.J. Jensen, I. Ragnarsson, L.L. Riedinger, H. Ryde, and P.O. Tjøm, Phys. Lett. B **406**, 193 (1997); **416**, 453(E) (1998).
[8] R.A. Bark, H. Carlsson, S.J. Freeman, G.B. Hagemann, F. Ingebretsen, H.J. Jensen, T. Lönnroth, M.J. Piiparinen, I. Ragnarsson, H. Ryde, H. Schnack-Petersen, P.B. Semmes, and P.O. Tjøm, Nucl. Phys. **A630**, 603 (1998).
[9] J.M. Espino, G.B. Hagemann, I.G. Bearden, R.A. Bark, M. Bergström, A. Bracco, B. Herskind, H.J. Jensen, S. Leoni, C. Martinez-Torre, B. Million, and P.O. Tjøm, Nucl. Phys. **A640**, 163 (1998).
[10] W. Reviol, L.L. Riedinger, X.Z. Wang, J.-Y. Zhang, H.J. Jensen, G.B. Hagemann, R.A. Bark, P.O. Tjøm, S. Leoni, T. Lönnroth, H. Schnack-Petersen, T. Shizuma, J. Wrzesinski, and P.B. Semmes, Phys. Rev. C **59**, 1351 (1999).

[11] D. Hojman, M.A. Cardona, D.R. Napoli, S.M. Lenzi, C.A. Ur, G. Lo Bianco, C.M. Petrache, M. Axiotis, D. Bazzacco, J. Davidson, M. Davidson, M. De Poli, G. De Angelis, E. Farnea, T. Kroell, S. Lunardi, N. Marginean, T. Martinez, R. Menegazzo, B. Quintana, and C. Rossi Alvarez, Eur. Phys. J. A **10**, 245 (2001).
[12] Y.H. Zhang, T. Hayakawa, M. Oshima, Y. Toh, J. Katakura, T. Komatsubara, and K. Furuno, Chin. Phys. Lett. **18**, 1323 (2001).
[13] Y.H. Zhang, M. Oshima, Y. Toh, M. Koizumi, A. Osa, T. Shizuma, T. Hayakawa, M. Sugawara, H. Kusakari, T. Morikawa, S.X. Wen, and L.H. Zhu, Eur. Phys. J. A **13**, 429 (2002).
[14] R.A. Bark, G.B. Hagemann, B. Herskind, H.J. Jensen, W. Korten, W. Wrzesinski, H. Carlsson, M. Bergström, A. Brockstedt, A. Nordlund, H. Ryde, P. Bosetti, S. Leoni, P. Tjøm, and F. Ingebretsen, Nucl. Phys. **A591**, 265 (1995).
[15] W.F. Mueller, H.Q. Jin, J.M. Lewis, W. Reviol, L.L. Riedinger, M.P. Carpenter, C. Baktash, J.D. Garrett, N.R. Johnson, I.Y. Lee, F.K. McGowan, C.-H. Yu, and S. Cwiok, Phys. Rev. C **59**, 2009 (1999).
[16] F.G. Kondev, M.P. Carpenter, R.V.F. Janssens, K. Abu Saleem, I. Ahmad, H. Amro, J.A. Cizewski, M. Danchev, C.N. Davids, D.J. Hartley, A. Heinz, T.L. Khoo, T. Lauritsen, C.J. Lister, W.C. Ma, G.L. Poli, J. Ressler, W. Reviol, L.L. Riedinger, D. Seweryniak, M.B. Smith, and I. Wiedenhöver, Phys. Lett. B **512**, 268 (2001).
[17] G.D. Dracoulis, B. Fabricius, T. Kibédi, A.M. Baxter, A.P. Byrne, K.P. Lieb, and A.E. Stuchbery, Nucl. Phys. **A534**, 173 (1991).
[18] B. Cederwall, B. Fant, R. Wyss, A. Johnsson, J. Nyberg, J. Simpson, A.M. Bruce, and J.N. Mo, Phys. Rev. C **43**, 2031 (1991).
[19] D.C. Radford. Nucl. Instrum. Methods Phys. Res. A **361**, 297 (1995).
[20] R.A. Bark, A.M. Baxter, A.P. Byrne, G.D. Dracoulis, T. Kibédi, T.R. McGoram, and S.M. Mullins, Nucl. Phys. **A691**, 577 (2001).
[21] J. Wauters, P. Dendooven, M. Huyse, G. Reusen, P. Van Duppen, R. Kirchner, O. Klepper, and E. Roecki, Z. Phys. A **345**, 21 (1993).
[22] U. Bosch, P. Koschel, W.-D. Schmidt-Ott, V. Freystein, T. Hild, F. Meissner, H. Salewski, U. Ellmers, and R. Michaelsen, Z. Phys. A **336**, 359 (1990).
[23] F. Rösel, H.M. Fries, F. Alders, and H.C. Pauli, At. Data Nucl. Data Tables **21**, 291 (1978).
[24] B. Fabricius, G.D. Dracoulis, R.A. Bark, A.E. Stuchbery, T. Kibédi, and A.M. Baxter, Nucl. Phys. **A511**, 345 (1990).
[25] G.D. Dracoulis, B. Fabricius, R.A. Bark, A.E. Stuchbery, D.G. Popescu, and T. Kibédi, Nucl. Phys. **A510**, 533 (1990).
[26] C.J. Gallagher and S.A. Moszkowski, Phys. Rev. **111**, 1282 (1958).
[27] R.A. Bark, S.W. Ødegård, R. Bengtsson, I.G. Bearden, G.B. Hagemann, B. Herskind, F. Ingebretsen, S. Leoni, H. Ryde, T. Shizuma, K. Strähle, P. Tjøm, and W. Wrzesinski, Phys. Rev. C **52**, R450 (1995).
[28] F. Dönau, Nucl. Phys. **A471**, 469 (1987).
[29] Benjamin E. Chi, Nucl. Phys. **83**, 97 (1966).
[30] G.D. Dracoulis, A.E. Stuchbery, A.P. Byrne, A.R. Poletti, S.J. Poletti, J. Gerl, and R.A. Bark, J. Phys. G **12**, L97 (1986).
[31] B. Cederwall, R. Wyss, A. Johnson, J. Nyberg, B. Fant, R. Chapman, D. Clarke, F. Khazaie, J.C. Lisle, J.N. Mo, J. Simpson, and I. Thorslund, Z. Phys. A **337**, 283 (1990).
[32] P.M. Davidson, G.D. Dracoulis, T. Kibédi, A.P. Byrne, S.S. Anderssen, A.M. Baxter, B. Fabricius, G.J. Lane, and A.E. Stuchbery, Nucl. Phys. **A567**, 219 (1999).
[33] S. Juutinen, P. Ahonen, J. Hattula, R. Julin, A. Pakkanen, A. Virtanen, J. Simpson, R. Chapman, D. Clarke, F. Khazaie, J. Lisle, and J.N. Mo, Nucl. Phys. **A526**, 346 (1991).
[34] R.A. Bark, S. Törmänen, T. Bäck, B. Cederwall, S.W. Ødegård, J.F.C. Cocks, K. Helariutta, P. Jones, R. Julin, S. Juutinen, H. Kankaapää, H. Kettunen, P. Kuusiniemi, M. Leino, M. Muikku, P. Rahkila, A. Savelius, A. Maj, M. Mattiuzzi, W. Mueller, L.L. Riedinger, and T. Saitoh, Nucl. Phys. **A657**, 113 (1999).
[35] R.A. Bark, J. Phys. G **17**, 1209 (1991).
[36] G.D. Dracoulis, B. Fabricius, A.P. Byrne, A.E. Stuchbery, A.M. Baxter, K.P. Lieb, K.J. Schiffer, and T. Kibédi, Phys. Lett. B **257**, 21 (1991).
[37] G.D. Dracoulis, B. Fabricius, T. Kibédi, A.P. Byrne, and A.E. Stuchbery, Nucl. Phys. **A554**, 439 (1993).
[38] R.A. Bark, R. Bengtsson, and H. Carlsson, Phys. Lett. B **339**, 11 (1994).
[39] Ragnar Bengtsson, Nucl. Phys. **A520**, 201c (1990).
[40] H.-Q. Jin, L.L. Riedinger, C.R. Bingham, M.P. Carpenter, V.P. Janzen, C.-H. Yu, L. Zhou, P.B. Semmes, J.-Y. Zhang, M.A. Riley, C. Baktash, M.L. Halbert, N.R. Johnson, I.Y. Lee, and F.K. McGowan, Phys. Rev. C **53**, 2106 (1996).
[41] R. Bengtsson and S. Frauendorf, Nucl. Phys. **A314**, 27 (1979); **A327**, 139 (1979).
[42] R.A. Bark, G.D. Dracoulis, and A.E. Stuchbery, Nucl. Phys. **A514**, 503 (1990).
[43] T. Bengtsson, Nucl. Phys. **A496**, 56 (1989).
[44] R. Bengtsson, T. Bengtsson, M. Bergström, H. Ryde, and G.B. Hagemann, Nucl. Phys. **A569**, 469 (1994).
[45] Jing-Ye Zhang, A.J. Larabee, and L.L. Riedinger, J. Phys. G **13**, L75 (1987).
[46] T. Bengtsson and Ingemar Ragnarsson, Nucl. Phys. **A436**, 14 (1985).
[47] Y.H. Zhang, T. Hayakawa, M. Oshima, Y. Toh, J. Katakura, Y. Hatsukawa, M. Matsuda, N. Shinohara, T. Ishii, H. Kusakari, M. Sugawara, and T. Komatsubara, Eur. Phys. J. A **8**, 439 (2000).
[48] G.B. Hagemann and I. Hamamoto, Phys. Rev. C **40**, 2862 (1989).
[49] W. Andrejtscheff, K.D. Schilling, and P. Manfrass, At. Data Nucl. Data Tables **16**, 515 (1975).
[50] M.A.J. Mariscotti, Gertrude Scharff-Goldhaber, and Brian Buck, Phys. Rev. **176**, 1864 (1968).
[51] H. Carlsson, M. Bergström, A. Brockstedt, L.P. Ekström, J. Lyttkens-Lindén, H. Ryde, R.A. Bark, G.B. Hagemann, J.D. Garrett, R. Chapman, D. Clarke, F. Khazaie, J.C. Lisle, and J.N. Mo, Nucl. Phys. **A551**, 295 (1993).
[52] H.J. Jensen, R.A. Bark, P.O. Tjøm, G.B. Hagemann, I.G. Bearden, H. Carlsson, S. Leoni, T. Lönnroth, W. Reviol, L.L. Riedinger, H. Schnack-Petersen, T. Shizuma, X.Z. Wang, and J. Wrzesinski, Nucl. Phys. **A695**, 3 (2001).